arXiv:1701.06133v1 [cond-mat.mes-hall] 22 Jan 2017

Chiral topological insulating phases from three-dimensional nodal loop semimetals

Linhu Li,[1,2] Chuanhao Yin,[3] Shu Chen,[3,4,5] and Miguel A. N. Araújo[1,2,6]

[1]*Beijing Computational Science Research Center, Beijing 100089, China*
[2]*CeFEMA, Instituto Superior Técnico, Universidade de Lisboa, Av. Rovisco Pais, 1049-001 Lisboa, Portugal*
[3]*Beijing National Laboratory for Condensed Matter Physics, Institute of Physics, Chinese Academy of Sciences, Beijing 100190, China*
[4]*School of Physical Sciences, University of Chinese Academy of Sciences, Beijing, 100049, China*
[5]*Collaborative Innovation Center of Quantum Matter, Beijing, China*
[6]*Departamento de Física, Universidade de Évora, P-7000-671, Évora, Portugal*

We identify a topological $\mathbb{Z}$ index for three dimensional chiral insulators with $P*T$ symmetry where two Hamiltonian terms define a nodal loop. Such systems may belong in the AIII or DIII symmetry class. The $\mathbb{Z}$ invariant is a winding number assigned to the nodal loop and has a correspondence to the geometric relation between the nodal loop and the zeroes of the gap terms. Dirac cone edge states under open boundary conditions are in correspondence with the winding numbers assigned to the nodal loops. We verify our method with the low-energy effective Hamiltonian of a three-dimensional material of topological insulators in the Bi_2Te_3 family.

PACS numbers: 03.65.Vf, 71.20.-b, 71.10.Fd

Introduction.- Topological insulators (TIs) in three dimensions (3D) having time reversal symmetry can be characterized by $\mathbb{Z}_2$ numbers defined on some discrete momenta[1–5], which is equivalent to a quantized invariant expressed as an integral over the entire Brillouin Zone (BZ)[6]. There are then two types of TI's, strong and weak, according to whether there is an odd or even number of Dirac cone surface states, respectively[5]. Besides the time reversal TIs, there is a class of chiral TIs which are described by a $\mathbb{Z}$-type topological invariant[7]. The geometrical representation of a topological invariant in some vector spaces provides an intuitive way to analyze the topological nature of many systems[8–12].

On the other hand, a transition point between topologically different insulating phases can be viewed as a semimetal phase with nontrivial topology in its gap closing points[13, 14]. Topological semimetals (TSMs)[15–21] have a Fermi surface (FS) with reduced dimension. While a 3D normal metal has a two-dimensional (2D) FS, a TSM has a one-dimensional (1D) or zero-dimensional (0D) FS at half-filling. 3D systems with 0D FS are known as the Weyl[15] or Dirac[16] semimetals. In these systems, the two bands touch linearly at discrete gap closing points in the BZ, and hold topologically protected edge states under open boundary conditions (OPC), such as for instance, the Fermi arcs. More recently, 3D nodal line semimetals[22–27] have attracted growing attention. In such systems, the linear band touching points form one or several 1D lines in the BZ.

One of the most interesting cases is when the nodal lines form closed, nodal loops (NLs). A NL can be classified in either of two classes, according to whether it carries a $\mathbb{Z}_2$ monopole charge or not. The one without a monopole charge can shrink into a point and disappear, and is topologically trivial in this sense. NLs are protected by the combination of inversion and time reversal symmetries, $P*T$, for spinless systems, while additional symmetries are required to protect NLs in 3D systems with spin-orbital coupling[26, 27]. On the other hand, NL semimetals have also been studied in 2D[28, 29]. In this case, although the NL itself does not carry topological charge, the addition of some chiral gap terms can make the system become topological and insulating, where the topological invariant is given by a winding number defined along the NL[29]. An interesting question to address is, what effect can gap terms have on a 3D NL semimetal?

In this paper, we study a spin-1/2 system with $P*T$ symmetry, and show that anticommuting mass gap terms can drive a 3D NL semimetal into a chiral TI, which can be characterized by a integer winding number defined along each NL. This winding number is determined by the geometric relation between the NL and the zeroes of the gap terms. Although the gap terms may be initially considered small, our results only depend on their zeroes, so that *it holds valid for any finite terms that gap out the NLs.* The system's surface states may hold an odd or even number of Dirac cones, and their existence has a correspondence to the NL winding number. In this sense, the NL can serves as an indicator of the topological properties of a 3D insulator. In order to show the utility of our theory, we apply it to a 3D material of the topological Bi_2Te_3 family and give a brief discussion.

Minimal model.- We begin our discussion with a simplest two band model for $P*T$ symmetry-protected NL semimetals:

$$H_0 = (m - k_x^2 - k_y^2)\sigma_x + k_z\sigma_z, \tag{1}$$

with σ the Pauli matrices acting on an orbital space. For spinless system, the $P*T$ symmetry is simply given by the complex conjugation and a unitary matrix, P, such that the Hamiltonian satisfies $PH_0^*(k)P^{-1} = H_0(k)$. In this case $P = 1$ and the $P*T$ symmetry ensures the absence of the second Pauli matrix. The nodes of H_0 yield a 1D solution, a NL with $k_z = 0$ and $k_x^2 + k_y^2 = m$. Introducing a σ_y term, $H = H_0 + h_y\sigma_y$, not only breaks $P*T$ symmetry but h_y also serves as an effective mass term, which can be either k-independent or related with k. In the former case, it opens a stable gap in the BZ, which drives the system into a trivial insulator. If h_y is a function of k, the nodes of H may be pairs of points, and the system is a

Weyl semimetal.

We extend this model by including the spin degree of freedom and write the Hamiltonian with $P*T$ symmetry as

$$H = H_0 + h_{yx}\sigma_y s_x + h_{yy}\sigma_y s_y + h_{yz}\sigma_y s_z, \quad (2)$$

where the Pauli matrices s_j act in spin space. $P*T$ symmetry now reads $Ps_yH_0^*(k)s_yP^{-1} = H_0(k)$, with $P = 1$ and satisfies $(P*T)^2 = -1$, Here we use the labels h_{ij} to represent the term of σ_i and s_j, with $i = 0$ or $j = 0$ for the identity matrix in the corresponding subspace. These five terms form an anticommuting set of Dirac matrices, but we note that there are also other equivalent choices[30]. The spectrum of (1)-(2) is simply given by

$$E_\pm = \pm\sqrt{h_{x0}^2 + h_{z0}^2 + h_{yx}^2 + h_{yy}^2 + h_{yz}^2}. \quad (3)$$

The effective mass gapping out the NL is now $|\mathbf{h}_y|$, where $\mathbf{h}_y = (h_{yx}, h_{yy}, h_{yz})$. Requiring $\mathbf{h}_y = 0$ may give a solution of points (0D), lines (1D) or surfaces (2D), depending on the number of non-zero k-dependent terms it has.

If $|\mathbf{h}_y|$ contains two non-zero k-dependent terms, $\mathbf{h}_y = 0$ shall give one or several 1D lines. Thus the system is generally an insulator, as the gap closing condition requires the crossing of the NL and these 1D lines, which is accidental. Such a four-component Dirac Hamiltonian describes a chiral topological insulator[7], as the model satisfies $SH(k)S^{-1} = -H(k)$, with the chiral operator S given by the absent fifth Dirac matrix. In the absence of time reversal symmetry, the system belongs to the AIII class and can be characterized by a Z invariant[3]. We define a winding number of $\mathbf{h}_y$ along the NL[29],

$$\nu_{NL} = \oint_{NL} \frac{h_2 dh_1 - h_1 dh_2}{|\mathbf{h}_y|^2}, \quad (4)$$

can be shown to be equivalent to a Berry phase of the occupied Bloch bands at half filling[31]. Here, h_1 and h_2 denote the two k-dependent terms of $\mathbf{h}_y$. If we consider the $k_x - k_y$ plane that contains the NL, the intersection of the 1D lines and the plane produces a series of singularities in the plane, and the winding number (4) of the NL is simply the summation of the windings around the singularities within the NL, as shown in Fig.1. This winding number may take on any integer value, as it is only associated with the number of lines going through the NL. We also note that in the presence of time reversal symmetry, this model would fall into the CII class, which is described by a Z_2 topological index instead[3].

Finally, if all the three terms of $\mathbf{h}_y$ are depended on k, $h_y = 0$ shall give one or several 0D points. In this case, the intersection of these points and the plane of the NL is also accidental. From the symmetry classification point of view, the presence of the fifth Dirac matrix breaks the chiral symmetry, and the model falls into the A class, which is non-topological in 3D. In other words, we could smoothly move a singularity out of the NL without closing the gap.

Winding numbers and geometry of the loops for a lattice model.- In order to reveal the topological properties described by the NL winding number, we next consider a lattice model described by an anticommuting set of Dirac matrices $\mathbf{\Gamma} = (\sigma_x s_0, \sigma_z s_0, \sigma_y s_x, \sigma_y s_y, \sigma_y s_z)$, as

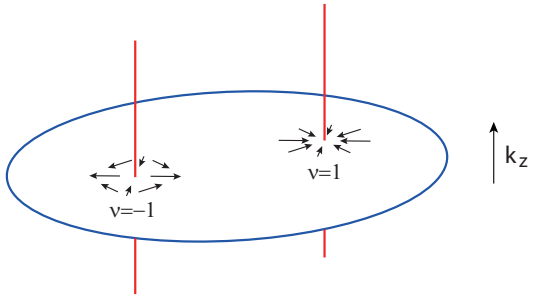

FIG. 1: A sketch of the winding number of a NL. The blue circle indicates the NL given by $H_0 = 0$, the red lines indicate the 1D solution of $\mathbf{h}_y = 0$ for models of the chiral class, and each line gives a singularity in the integrand of (4) in the NL plane. The arrows around each singularity show the direction of $\mathbf{h}_y$ near this point, and the corresponding winding number of these points are labeled in the sketch. The winding number of the NL, ν_{NL}, is given by the summation of winding numbers of every singularity within the NL, as the integral path can be smoothly transformed into circles around each singularity.

$$H = \mathbf{h}(k)\cdot\mathbf{\Gamma}, \quad (5)$$

with

$$\begin{aligned}\mathbf{h}(k) &= (h_{x0}, h_{z0}, h_{yx}, h_{yy}, h_{yz}),\\ h_{x0} &= \mu - t_\parallel(\cos k_x + \cos k_y),\\ h_{z0} &= -t_\perp \cos k_z,\end{aligned}$$

which form two NLs in $k_x - k_y$ plane for $k_z = \pi/2$ and $-\pi/2$ when $0 < |\mu/t_\parallel| < 2$. The position and shape of the NLs are only associated with the ratio of μ and $t_\parallel$, hence we can choose $t_\parallel = t_\perp = 1$ for the sake of simplicity. In the following we only consider the case with positive μ, with the center of the NLs given by $k_x = k_y = 0$. For negative μ, the center of the NLs is at $k_x = k_y = \pi$, and a similar discussion applies. The two NLs of $k_z = \pm\pi/2$ give two independent winding numbers, $\nu_{NL}^\pm$, respectively, and we define the total winding number of the system as

$$\nu_{sum} = \nu_{NL}^+ + \nu_{NL}^-. \quad (6)$$

Without loss of generality, here we choose $h_{yx} = 0$ to preserve a chiral symmetry with the operator $S = \sigma_y s_x$. The other two gap terms of $\mathbf{h}_y$ are functions of k, and $\mathbf{h}_y = 0$ gives 1D lines in the BZ. We consider the following form of $\mathbf{h}_y$ that breaks time reversal symmetry:

$$h_{yy} = -t_y \sin k_y \quad (7)$$

$$h_{yz} = \mu_s - t_x \sin k_x - t_z \sin k_z, \quad (8)$$

and the system falls into the AIII class. $|\mathbf{h}_y| = 0$ gives some 1D lines in the $k_x - k_z$ plane with $k_y = 0$ or π, which may or may not be enclosed by the NLs. We would also like to point

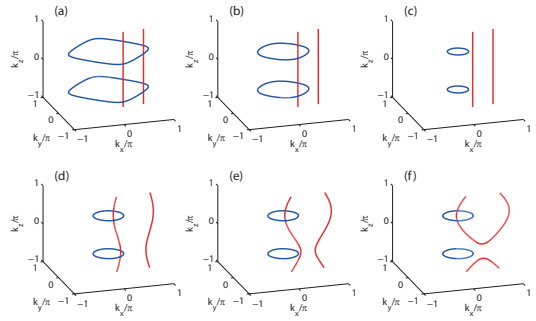

FIG. 2: The NLs and the 1D lines given by $|\mathbf{h}_y| = 0$, represented by blue and red lines respectively. For the latter, we only show the lines with $k_y = 0$, as the ones for $k_y = \pi$ lie outside the NLs. (a) $\mu = 0.2$, $\mu_s = 0.8$ and $t_z = 0$; (b) $\mu = 1$, $\mu_s = 0.8$ and $t_z = 0$; (c) $\mu = 1.8$, $\mu_s = 0.8$ and $t_z = 0$; (d) $\mu = 1.6$, $\mu_s = 0.5$ and $t_z = 0.2$; (e) $\mu = 1.6$, $\mu_s = 0.5$ and $t_z = 0.4$; (f) $\mu = 1.6$, $\mu_s = 0.5$ and $t_z = 0.6$.

out that although the gap terms need be small for the system to preserve a NL like structure, *the topological properties are not related to the exact value of these terms, but only to the ratios between them*. For the sake of simplicity, we choose $t_y = t_x = 1$ and positive μ_s hereafter.

We first consider a simple case with $t_z = 0$. In this case, the 1D solution of $\mathbf{h}_y = 0$ gives four lines perpendicular to $k_x - k_y$ plane, two with $k_y = 0$ and two with $k_y = \pi$. For positive μ, the pair of lines with $k_y = \pi$ are always outside the loop. By tuning μ_s and μ, the NLs may enclose 2, 1 or 0 lines with $k_y = 0$, as shown by Fig.2(a)-(c). However, the windings of these lines in the $k_x - k_y$ plane have opposite values (as in Fig.1), and the NL enclosing either 0 or 2 lines will result in $\nu_{NL} = 0$. On the other hand, as the system preserves a reflection symmetry along z direction, each line will be enclosed by either two or none of the NLs, hence the total winding number, ν_{sum}, in this case is always even.

In the presence of a nonzero t_z, the reflection symmetry is broken, and the lines of $|\mathbf{h}_y| = 0$ will change shape with t_z and eventually form a closed ring, as shown in Fig.2(d)-(f). In this case, an enclosed line will cross one of the NLs at some point, resulting in a topological phase transition. After this transition, the system has an odd winding number, $\nu_{sum} = 1$, as only one of the NLs encloses a singularity.

edgestates and phase diagram.- The topological properties of a 3D topological insulator can be represented by the number of Dirac cones in the edge states under OBC. Next, we apply the method in Ref.[32] to study the edge states in our model. The existence of edge states and their eigenenergies, under OBC, are associated with the bulk topology of the system, which can be seen by the trajectory of $\mathbf{h}(k)$ in the 5-component vector space formed by the Dirac matrices $\mathbf{\Gamma}$. Here we choose a surface plane perpendicular to the x direction by fixing k_y and k_z, and study the corresponding edge states as an example. Edge states in the other two directions can also be studied in this way, and give similar results are obtained. The Hamiltonian terms associated with k_x give an elliptical trajectory of $\mathbf{h}$ in the 1-5 plane in $\mathbf{\Gamma}$ space,

$$\mathbf{h}(k_x) = (-\cos k_x, 0, 0, 0, -\sin k_x). \tag{9}$$

The remaining Hamiltonian terms,

$$\mathbf{h}^0 = (\mu - \cos k_y, -\cos k_z, 0, -\sin k_y, \mu_s - t_z \sin k_z), \tag{10}$$

can be viewed as the vector from the origin of the vector space to the center of the ellipse $\mathbf{h}(k_x)$. The parallel and perpendicular components of $\mathbf{h}^0$ to the 1-5 plane are given by

$$\mathbf{h}^0_{\parallel} = (\mu - \cos k_y, 0, 0, 0, \mu_s - t_z \sin k_z), \tag{11}$$

$$\mathbf{h}^0_{\perp} = (0, -\cos k_z, 0, -\sin k_y, 0). \tag{12}$$

The existence of edge states depends on whether the ellipse $\mathbf{h}(k_x)$ encloses the point $\mathbf{h}^0_{\parallel}$, and this condition reads

$$|\mathbf{h}^0_{\parallel}| = \sqrt{(\mu - \cos k_y)^2 + (\mu_s - t_z \sin k_z)^2} < 1. \tag{13}$$

Provided that Eq.(13) holds, the edge state energies are given by

$$E_{\pm} = |\mathbf{h}^0_{\perp}| = \pm\sqrt{\cos^2 k_z + \sin^2 k_y}. \tag{14}$$

Candidate Dirac cones at $(k_y, k_z) = (0, \pm\frac{\pi}{2})$ must satisfy the inequality (13). When $t_z = 0$, Eq.(13) becomes

$$(\mu - 1)^2 < 1 - \mu_s^2, \tag{15}$$

for both $k_z = \pm\frac{\pi}{2}$. In other words, it gives either no Dirac cone, or a pair of Dirac cones at $(k_y, k_z) = (0, \pm\frac{\pi}{2})$. For nonzero t_z, there may exist 0, 1 or 2 Dirac cones depending on the parameters, as the condition (13) becomes

$$(\mu_s \mp t_z)^2 < 2\mu - \mu^2, \tag{16}$$

for $k_z = \pm\frac{\pi}{2}$, respectively. In Fig.2 we display phase diagrams showing the number of Dirac cone edge states. These results are also in consistence with the winding numbers of the NLs, as shown in the figure.

In order to visualize the edge states, next we choose open boundary condition in x direction and rewrite the Hamiltonian as a tight-binding between planes

$$H = \sum_n \hat{c}_n^{\dagger} U_d \hat{c}_n + \sum_n \frac{1}{2} \hat{c}_{n+1}^{\dagger} U_{od} \hat{c}_n + h.c., \tag{17}$$

with $\hat{c}_n$ is a vector of annihilation operators $\hat{c}_{n,\sigma,s}$ on plane n, $\hat{c}_n = (\hat{c}_{n,+,+}, \hat{c}_{n,+,-}, \hat{c}_{n,-,+}, \hat{c}_{n,-,-})_n$, and

$$U_d = (\mu - \cos k_y)\sigma_x s_0 - \cos k_z \sigma_z s_0 - \sin k_y \sigma_y s_y + (\mu_s - t_z \sin k_z)\sigma_y s_z, \tag{18}$$

$$U_{od} = -\sigma_x s_0 + i\sigma_y s_z. \tag{19}$$

We numerically diagonalize this Hamiltonian and show the four closest doubly degenete energy bands above and below

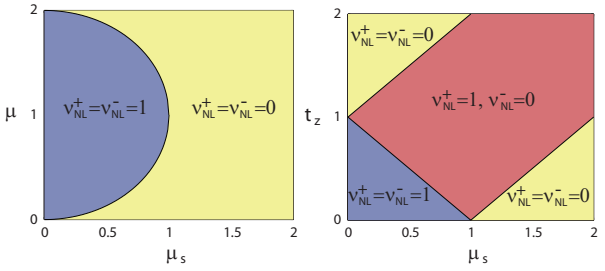

FIG. 3: Phase diagram with $t_z = 0$ (left) and $\mu = 1$ (right). The number of Dirac cones in edge states equals to the total winding number of the model, $\nu_{sum} = \nu^+_{NL} + \nu^-_{NL}$. In the left panel, the yellow region with $\nu^+_{NL} = \nu^-_{NL} = 0$ includes three different situations: i) two lines are enclosed by the NLs when $\mu_s < 1$ and $\mu < 1$; ii) all the lines are out of the NLs when $\mu_s < 1$ and $\mu > 1$; and iii) not any line exsits when $\mu_s > 1$.

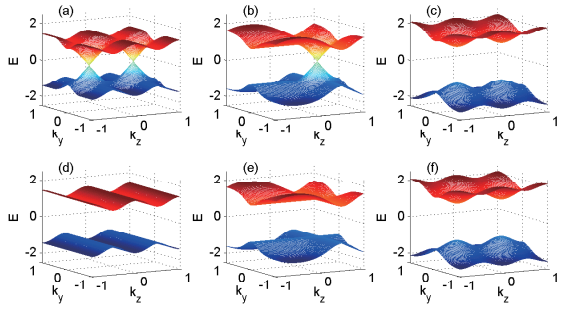

FIG. 4: The spectra of the two doublet bands nearest to $E = 0$, (a)-(c) for open boundary condition along x, and (d)-(f) for period boundary condition. The three columns are for three topologically different phases, while the left two are topologically nontrivial. The parameters are $\mu = 1$ and (a), (d) $\mu_s = t_z = 0$; (b), (e) $\mu_s = t_z = 1$; and (c), (f) $\mu_s = 2$, $t_z = 0$.

zero energy in Fig.4, with OBC along x from (a) to (c), and periodic boundary condition from (d) to (f) as comparison. Panels (a) and (b) are for the topologically nontrivial phases with $\nu^+_{NL} = \nu^-_{NL} = 1$ and $\nu^+_{NL} = 1$, $\nu^-_{NL} = 0$, and the spectra show edge states with two or one Dirac cone, respectively. Panel (c) is for the topologically trivial phase with $\nu^+_{NL} = \nu^-_{NL} = 0$, where there is no edge state connecting the conduction and valence bands.

A real material example.-Finally, we apply our method to 3D topological insulators of the Bi_2Te_3 family[33]. These materials possess time reversal symmetry and are characterized by a Z_2 number. Nevertheless, their topological nature is determined by the physics near the time-reversal-invariant point $\Gamma(0,0,0)$ in the Brillouin zone, around which the low-energy effective Hamiltonian also satisfies a chiral symmetry. This Hamiltonian is given by

$$H(k) = \epsilon_0(k) I_{4\times4} + \begin{pmatrix} M(k) & A_1 k_z & 0 & A_2 k_- \\ A_1 k_z & -M(k) & A_2 k_- & 0 \\ 0 & A_2 k_+ & M(k) & -A_1 k_z \\ A_2 k_+ & 0 & -A_1 k_z & -M(k) \end{pmatrix}, \quad (20)$$

with $k_\pm = k_x \pm i k_y$, $\epsilon_0(k) = C + D_1 k_z^2 + D_2 |k_+|^2$ and $M(k) = M - B_1 k_z^2 - B_2 |k_+|^2$. Using Dirac matrices, this Hamiltonian can be written as

$$H(k) = M(k)\sigma_z s_0 + A_1 k_z \sigma_x s_z + A_2 k_x \sigma_x s_x + A_2 k_y \sigma_x s_y, \quad (21)$$

where we left out the identity matrix as it only changes the shape of the energy bands, not the topology of the system. The chiral operator is given by the absent fifth Dirac matrix, $S = \sigma_y s_0$.

$P * T$ symmetry is here implemented by $P = \sigma_z$. However, we note that particle-hole symmetry also exists in this case, which reads $CH^*(-k)C^{-1} = -H(k)$, with $C = \sigma_y s_y$, and satisfies $CC^* = 1$. Thus the model Eq.(21) falls into the DIII class, which is also characterized by a Z invariant in 3D[3]. Similar to our previous discussion, we write $H = H_1 + H_2$, with

$$H_1(k) = M(k)\sigma_z s_0 + A_1 k_z \sigma_x s_z \,, \quad (22)$$

$$H_2(k) = A_2 k_x \sigma_x s_x + A_2 k_y \sigma_x s_y \,. \quad (23)$$

Then H_1 has a NL in $k_x - k_y$ plane, and the nodes of H_2 produce a single line enclosed by the loop. This gives a NL winding number $\nu_{NL} = 1$, which corresponds to the topological properties of the Γ point.

Summary.- In summary, we have studied Hamiltonians with $P * T$ symmetry where two terms define a NL which is gapped out by the other terms. In the presence of chiral symmetry, these gap terms can drive the system into a chiral TI, which can be described by a winding number defined along the NL. This winding number is associated with the geometric relation between the NL and the zeroes of the gap terms. We investigated a lattice model in detail, which has two NLs in the BZ, each of them with a winding number of 1 or 0 due to the gap terms. This winding number corresponds to the emergence of a Dirac cone for the surface states under OBC. Finally, we applied our method to the 3D topological insulators of the Bi_2Te_3 family, and showed the connection between their topological nature and the NL winding number.

Acknowledgments.- Financial support from FCT through grant UID/CTM/04540/2013 is acknowledged. S. C. is supported by NSFC under Grants No. 11425419, No. 11374354 and No. 11174360.

[1] M.Z. Hasan and C.L. Kane, Rev. Mod. Phys. **82**, 3045 (2010).
[2] X.L. Qi and S.C. Zhang, Rev. Mod. Phys. **83**, 1057 (2011).
[3] A. P. Schnyder, S. Ryu, A. Furusaki, and A.W.W. Ludwig, Phys. Rev. B **78**, 195125 (2008);
[4] J. E. Moore and L. Balents, Phys. Rev. B **75**, 121306 (2007).
[5] L. Fu, C. L. Kane, and E. J. Mele, Phys. Rev. Lett. **98**, 106803 (2007).
[6] Z. Wang, X.-L. Qi, and S.-C. Zhang, New Journal of Physics **12**, 065007 (2010).
[7] P. Hosur, S. Ryu, and A. Vishwanath, Phys. Rev. B **81**, 045120 (2010).
[8] P. Delplace, D. Ullmo, and G. Montambaux, Phys. Rev. B **84**, 195452 (2011).

[9] G. Zhang, Z. Song, Phys. Rev. Lett. **115**, 177204 (2015).
[10] L. Li and S. Chen, Phys. Rev. B **92**, 085118 (2015).
[11] L. Li, C. Yang, S. Chen, Europhys. Lett. **112**, 10004 (2015).
[12] L. Li, C. Yang, S. Chen, Eur. Phys. J. B (2016) 89: 195.
[13] B.-J. Yang, N. Nagaosa, Nature Communications, **5**, 4898 (2014).
[14] S. Ganeshan, S. Das Sarma, Phys. Rev. B **91**, 125438 (2015).
[15] X.Wan, A.M. Turner, A. Vishwanath, and S. Y. Savrasov, Phys. Rev. B **83**, 205101 (2011).
[16] S. M. Young, S. Zaheer, J. C. Y. Teo, C. L. Kane, E. J. Mele, and A. M. Rappe, Phys. Rev. Lett. **108**, 140405 (2012).
[17] P. Delplace, J. Li, and D. Carpentier, Europhys. Lett. **97**, 67004 (2012).
[18] J-.M. Hou, Phys. Rev. Lett. **111**, 130403 (2013).
[19] T. Morimoto and A. Furusaki Phys. Rev. B **89**, 235127 (2014).
[20] S. M. Young and C. L. Kane, Phys. Rev. Lett. **115**, 126803 (2015).
[21] S. Ganeshan and S. Das Sarma, Phys. Rev. B **91**, 125438 (2015).
[22] A. A. Burkov, M. D. Hook, and Leon Balents, Phys. Rev. B **84**, 235126 (2011).
[23] K. Mullen, B. Uchoa, and D. T. Glatzhofer, Phys. Rev. Lett. **115**, 026403 (2015).
[24] R. Nandkishore, Phys. Rev. B **93**, 020506 (2016).
[25] Z. Yan and Z. Wang, Phys. Rev. Lett. **117**, 087402 (2016).
[26] C. Fang, Y. Chen, H.-Y. Kee, and L. Fu, Phys. Rev. B **92**, 081201 (2015).
[27] C. Fang, H. Weng, X. Dai, and Z. Fang, Chinese Phys. B **25**, 117106 (2016).
[28] J. L. Lu, W. Luo, X. Y. Li, S. Q. Yang, J. X. Cao, X. G. Gong, and H. J. Xiang, arXiv:1603.04596.
[29] L. Li, M. A. N. Araújo, Phys. Rev. B **94**, 165117 (2016).
[30] Arfken, G. Mathematical Methods for Physicists, 3rd ed. Orlando, FL: Academic Press, pp. 211-217, (1985).
[31] M. V. Berry, Proc. R. Soc. London, Ser. A **392**, 45 (1984).
[32] R. S. K. Mong and V. Shivamoggi, Phys. Rev. B **83**, 125109 (2011).
[33] H. Zhang, C.-X. Liu, X.-L. Qi, X. Dai, Z. Fang and S.-C. Zhang Nat. Phys. **5**, 438 (2009).